Chapter 3
SMOS and Aquarius/SAC-D Missions: The Era of Spaceborne Salinity Measurements is About to Begin

Gary Lagerloef and Jordi Font

3.1 Introduction

During the Oceans from Space Venice 2000 meeting a decade ago, a friendly wager was made among a few participants. The potential for salinity measurement from space was a topic of lively discussion at a Special Session on Salinity Remote Sensing. There were some promising developments presented indicating that this capability would be achieved during decade ahead. The European Space Agency (ESA) pathfinder Soil Moisture Ocean Salinity (SMOS) mission had been selected in 1999. Meanwhile, NASA scientists were actively planning a pathfinder salinity mission proposal for a mid-2001 deadline, eventually to be named Aquarius. It was then estimated that these missions would be launched as early as mid-decade. Some participants were quite skeptical. After all, the scientific accuracy required is ~0.2 pss (practical salinity scale 1978), which equates to about ½ pinch of salt in a bottle of wine. So the wager was made, with a bottle of wine at stake, whether or not satellite-based salinity measurements would be presented at Oceans for Space 2010.

The wager's outcome is still unresolved, and will be decided at the 2010 meeting, although the odds may slightly favor the proponents. SMOS was launched successfully into orbit November 2nd, 2009. After a lengthy checkout period, preliminary data will be available to the science validation team about 2 months prior to the Oceans from Space 2010 meeting. Every effort will be made to have some preliminary results to show. Meanwhile, the Aquarius/SAC-D mission, a partnership between NASA and Argentina is now planned for launch in the Fall 2010, several months after the Oceans from Space 2010 meeting.

The past decade clearly has seen major progress, both technically and scientifically, toward meeting the challenge of measuring ocean salinity from space. This paper presents some of the history of this decade of progress, by describing the development of the SMOS and Aquarius/SAC-D missions and their scientific capabilities. The timely completion and launch of these satellite missions indicates that

G. Lagerloef (✉)
Earth and Space Research, Seattle, WA 98121, USA
e-mail: Lager@esr.org

V. Barale et al. (eds.), *Oceanography from Space*,
DOI 10.1007/978-90-481-8681-5_3,

the year 2010 marks the turning point that will begin the era of space borne salinity measurements.

3.2 Scientific Background – Links Between the Ocean Circulation, Water Cycle and Climate

The 1990s saw a confluence of two important developments for sea surface salinity (SSS) remote sensing. Scientifically, there was increasing awareness of the connection between surface salinity, ocean circulation and climate variability (e.g. Broecker, 1991). Meanwhile, advances in microwave radiometer technology were making it feasible to measure SSS at the levels of accuracy, spatial and temporal resolution needed to address important scientific questions (Lagerloef et al., 1995). By the time of Oceans from Space 2000, the key scientific themes had been identified for applying satellite SSS data study the links to ocean circulation and climate. These included tropical air sea interactions and El Niño, high-latitude convection and salinity anomalies, mid-latitude subduction processes, and the relation of salinity to changes in the global water cycle. The mission concepts were evolving to address these topics with measurement capabilities of ∼0.2 pss accuracy on ∼100–200 km and 10–30 day resolutions.

Scientific interest continued to grow during the past decade, reflected, for example, in the *Journal of Geophysical Research* special section on ocean salinity (Lagerloef, 2002). This included about two dozen peer-reviewed papers addressing the role of SSS on upper ocean dynamics, air-sea interaction and climate based on observational and modeling studies. Ocean salinity's critical importance to understanding and predicting climate variability was further documented in the report of the US CLIVAR Salinity Working Group (US CLIVAR, 2007) and the Intergovernmental Panel on Climate Change (IPCC, 2007).

These assessments identified salinity variability as a key index of the marine hydrologic cycle. SSS is a tracer for varying evaporation and precipitation, runoff and ice processes. These have important consequences for oceanic currents and mixing dynamics that influence the ocean's capacity to absorb, transport and store heat, freshwater and carbon dioxide. The assessments also reviewed clear observational evidence of decades-long changes, for example, of decreasing salinity in the subpolar North Atlantic and Southern Ocean, while the near surface salinity in the subtropics was increasing.

More recent studies reveal new features in these trends and links to water cycle, circulation and anthropogenic climate change. Stott et al. (2008) attributed to human influence the recent increases in the observed salinity in the Atlantic (20–50°N). Gordon and Giulivi (2008) found opposing trends, increasing since the late-1980s, in the sub-tropical gyres of North Atlantic and North Pacific, with the latter experiencing a relative freshening (Fig. 3.1). The authors attributed this to increasing atmospheric transport of fresh water from Atlantic to Pacific via the trade winds across Central America. The North Atlantic and Nordic Seas upper ocean freshening trend of the 1960s–1990s has reversed over the last decade (Holliday et al., 2008). This may be attributed to changes in the ocean circulation (Hakkinnen and

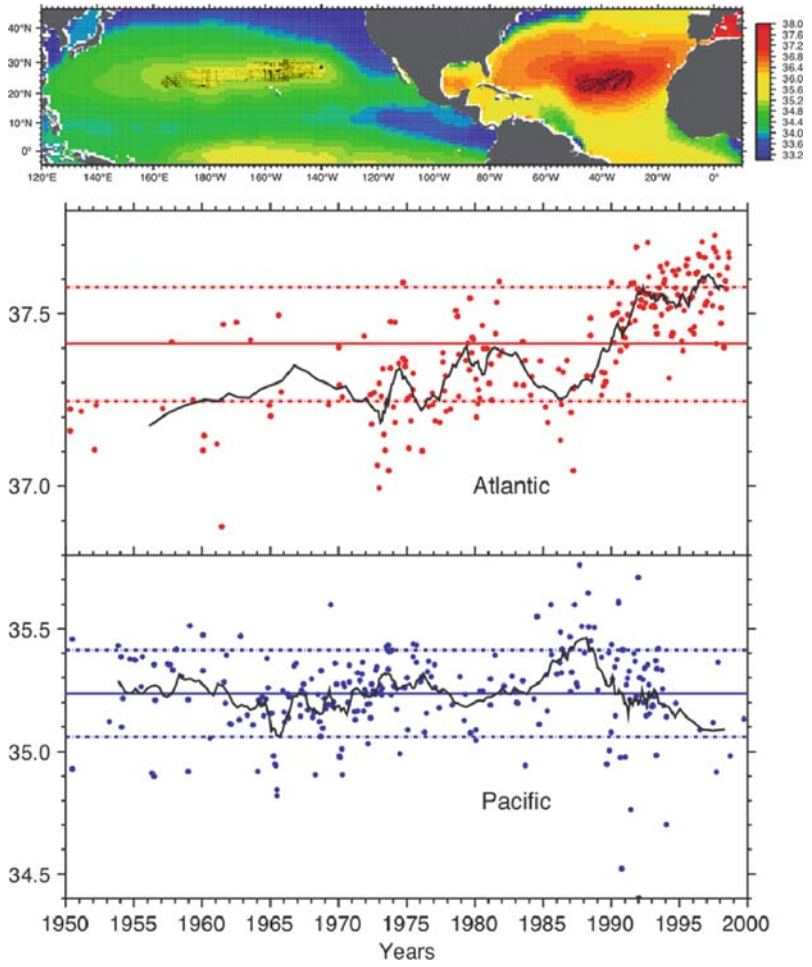

Fig. 3.1 Recently documented inversely correlated surface salinity trends in Atlantic and Pacific subtropical gyres, consistent with increasing atmospheric water transport from the Atlantic to Pacific (from Gordon and Giulivi, 2008)

Rhines, 2009), whereby warm and salty subtropical waters increased their penetration toward the Nordic seas. This suggests that salinity trends are related to changes in ocean circulation as well as the hydrologic cycle, and these different linkages need to be resolved.

Many of the fundamental processes involving salinity in the modulation of upper-ocean circulation and mixing remain poorly understood in both tropical and high-latitude regions. Nor are they adequately represented in climate models, and yet model studies do indicate that expanded monitoring of salinity (both satellite and in-situ) will measurably improve climate forecasts on inter-annual to decadal timescales (US Clivar, 2007).

3.3 Basic Principles and Issue for Salinity Remote Sensing

Salinity remote sensing is possible because the microwave emission of the sea surface at a given radio frequency depends partly on the dielectric coefficient of sea water, which in turn is partly related to salinity and temperature (Klein and Swift, 1977; Meissner and Wentz, 2003). The total power of the emission at horizontal (H) and vertical (V) polarization is measured remotely with a microwave radiometer. The output is given in terms of a parameter called brightness temperature (T_{BH} and T_{BV}) at each polarization, which are respectively the products of the surface emissivities (e_{H} and e_{V}) and the absolute temperature of the sea surface (T):

$$\begin{aligned} T_{\mathrm{BH}} &= e_{\mathrm{H}} T \\ T_{\mathrm{BV}} &= e_{\mathrm{V}} T \end{aligned} \tag{3.1}$$

The polarized emissivity for a flat sea (no wind/wave roughness), given by Equation (3.2), is governed by Fresnel reflection, the dielectric coefficient (ε), and the viewing angle from nadir (θ) (e.g. Swift and McIntosh, 1983).

$$\begin{aligned} e_{\mathrm{H}} &= 1 - \left[\frac{\cos\theta - (\varepsilon - \sin^2\theta)^{1/2}}{\cos\theta + (\varepsilon - \sin^2\theta)^{1/2}} \right]^2 \\ e_{\mathrm{V}} &= 1 - \left[\frac{\varepsilon\cos\theta - (\varepsilon - \sin^2\theta)^{1/2}}{\varepsilon\cos\theta + (\varepsilon - \sin^2\theta)^{1/2}} \right]^2 \end{aligned} \tag{3.2}$$

The above equations apply to all emitting surfaces, including seawater. At $\theta = 0$, both polarizations are the same.

Salinity (S) and temperature (T) enter the formulation through the complex dielectric coefficient ε, which depends on the microwave radio frequency (f), the electrical conductivity of sea water $C(S,T)$ and other factors, some of which are also dependent on (S,T). Klein and Swift (1977) is perhaps the most commonly applied model and is theoretically based on a simplified Debye equation and fitted with laboratory measurements of the dielectric coefficient. However, there are uncertainties in this model and additional studies have been carried out in recent years, including Blanch and Aguasca (2004), Meissner and Wentz (2003), Strogryn (1997), and Ellison et al. (1998), which all have inconsistencies relative to one-another. Differences among these models were evaluated by Wilson et al. (2004) in comparison to carefully controlled H and V polarization microwave brightness temperature measurements at $f = 1.413$ GHz (the L-band frequency to be used for measuring salinity). The Klein–Swift and the Meissner–Wentz models generally agreed the best with the brightness temperature observations, with uncertainties of between 0.02 and 0.07 K, whereas the others showed significant trends over the expected ranges of temperature and salinity. While these uncertainties are of similar magnitude to other terms in the error budgets (see below), this model function error is an important concern, and because the dielectric coefficient is a fundamental physical property of seawater, it should be know as accurately as possible. A

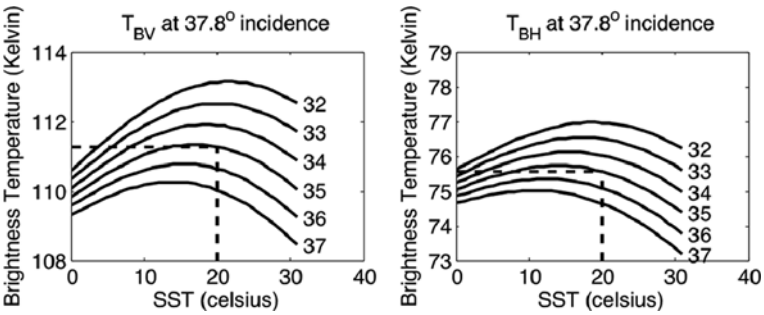

Fig. 3.2 Brightness Temperatures T_{BV} (*left*) and T_{BH} (*right*) as a function of SSS (contours) and SST (abscissa) for typical ocean surface conditions, and incidence angle of 37.8° (as an example from one of the Aquarius/SAC-D satellite viewing angles). Salinity can be determined from either polarization when SST is known (*dashed lines*). Calculations based on the dielectric model Klein and Swift (1977)

new set of laboratory measurements is presently being carried out (Lang, 2008). The dielectric model, combined with in-situ SSS and SST validation measurements will provide a consistent calibration reference for present and future salinity satellite missions.

Satellite remote sensing of salinity is done in the protected L-band frequency centered at 1.413 GHz to avoid radio interference. At this band, the brightness temperature change relative to a change in salinity, although small, is nevertheless enough to make SSS remote sensing possible, given sufficiently sensitive radiometric measurements. Figure 3.2 shows the relationship between T_{BH} and T_{BV} with SST and SSS for a particular viewing angle. The contour lines are for salinities ranging from 32 to 37 psu. It is easy to see that a unique value of salinity can be retrieved when SST and either T_{BH} or T_{BV} are known. This is the essence of how salinity remote sensing is achieved, although it is more complicated in practice. The SMOS and Aquarius instruments approach the salinity retrieval in very different ways, based on sensor design, as will be explained further below.

The dynamic range of brightness temperature is about 5 K over the range of typical open ocean surface salinity and temperature conditions. At a given temperature, brightness temperature decreases as salinity increases, whereas the tendency with respect to temperature changes sign. The salinity contours are spread farther apart for V polarization than for H, and therefore V is slightly more sensitive to salinity changes. The sensitivity is strongly affected by temperature, being largest at the highest temperatures and yielding better measurement precision in warm versus cold ocean conditions. Corrected brightness temperature will need to be measured to 0.02–0.08 K precision to achieve 0.1 pss salinity resolution. The difference in sensitivity between polarizations also increases with incidence angle (not shown). Temporal and spatial averaging can reduce random error. The degraded measurement precision in higher latitudes will be partly offset by averaging with the greater sampling frequency from a polar orbiting satellite.

Other sources of error in the SSS retrieval include numerous effects that change the brightness temperatures from the idealized flat surface emmission in Equations (3.1) and (3.2) to what is actually measured by a satellite radiometer in orbit. These include surface reflections of astronomical L-band radiation sources such as the cosmic background, galactic core, sun and moon. Attenuation in the atmosphere and ionosphere, including Faraday rotation (Yueh, 2000) must also be corrected. Clouds are transparent at L-band and pose not problem, but attenuation during very heavy rain can be significant and those data will need to be flagged. The T_B variation with respect to temperature falls generally between $\pm 0.15\,K°C^{-1}$ and near zero over a broad S and T range. Knowledge of the surface temperature to within a few tenths °C will be adequate to correct T_B for temperature effects and can be obtained using data from other satellite systems. In general these terms are well understood and will be corrected with appropriate models and ancillary data. See Lagerloef et al. (2008) for these terms tabulated for the Aquarius error analysis. The optical depth for this microwave frequency in seawater is about 1–2 cm, and the remotely sensed measurement depends on the T and S in that surface layer thickness, which poses a potential problem when comparing satellite data to in-situ measurements within a few meters of the surface.

The error source posing the most significant problem, however, is the change in emissivity from surface roughness due to wind, including sea state, wave breaking and foam. The change in T_B due to wind is much smaller at L-band than at higher frequencies (Hollinger, 1971), but nevertheless it is still the largest error source for salinity remote sensing. The Wind and Salinity Experiment (WISE) field study early in the decade (Camps et al., 2004; Gabarró et al., 2004) measured the L-band response wind, wave height and foam at a range of incidence angles and developed empirical formulas relative to those variables. These results show that the T_{BH} response is much larger than T_{BV} for incidence angles from 25 to 65° and is typically 0.2–0.4 K/m/s of wind. This implies large corrections for even moderate winds of a few m/s. Recent airborne measurements show that the T_{BV} response is larger than indicated by the WISE data, and that there is a detectable modulation due to the wind direction in both polarizations (S. Yueh, 2009, personal communication). Clearly there remains considerable uncertainty in correcting the wind and roughness effect, and this will be addressed once the satellites are on orbit through the calibration and validation activities. The Aquarius instrument will use radar backscatter to help make this correction, where as SMOS will derive a wind correction through a complex inversion algorithm that will rely on a model such as WISE that covers the full range of SMOS incidence angles.

3.4 Soil Moisture Ocean Salinity (SMOS) Mission

3.4.1 Early Configuration and Evolution of Design

ESA organized in 1995 a consultative meeting on “Soil Moisture and Ocean Salinity, Measurement Requirements and Radiometer Techniques” to analyze the feasibility

of low microwave passive remote sensing for the measurement of these two geophysical variables (Kerr et al., 1995). Besides confirming L-band radiometry as a viable option, it was concluded that the most promising technique to address the requirements for a simultaneous acquisition of both parameters was interferometric aperture synthesis radiometry, a concept developed in the 1950s to obtain high resolution radio images of celestial bodies and that had been demonstrated to be useful for Earth observation (Ruf et al., 1988). The interferometry design, inspired from the very large baseline antenna concept, consists of deploying small receivers in space, then reconstructing a brightness temperature (T_B) field through Fourier synthesis in a snapshot basis with a resolution corresponding to the spacing between the outmost receivers (Fig. 3.3).

A synthetic aperture radiometer measures all cross-correlation products between the signal pairs collected by the array elements (Corbella et al., 2004) and the total

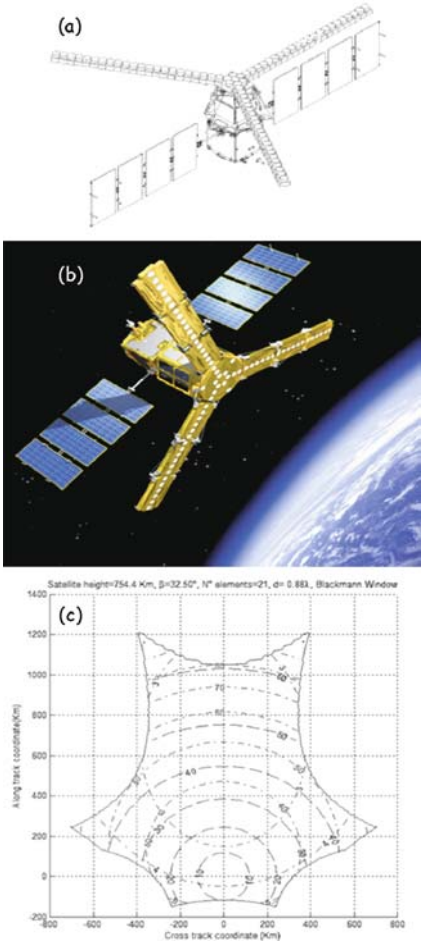

Fig. 3.3 (**a**) The initially proposed SMOS L-band plus C-band satellite in flight configuration (SMOS proposal to ESA). (**b**) Artist's view of the final SMOS configuration, with the 3 antenna arms of the MIRAS instrument and the PROTEUS platform with its solar panels deployed (ESA). (**c**) The SMOS instantaneous AF-FOV (*irregular curved hexagon*) with variable pixel characteristics: incidence angle (*dashed lines*) ranges from 0 to 65°, spatial resolution (*dash-dotted lines*) from 32 to 100 km, and expected radiometric sensitivity (*dash-dotted*) from 2.5 K at boresight to 5 K (generated by the SMOS end-to-end Performance Simulator)

power of the scene is also measured using at least one real aperture radiometer connected to one of the antennas. The relatively high spatial resolution (less than 50 km) and the short revisit time (1–3 days) imposed by soil moisture science objectives, are more feasible at this low frequency with such a new approach than with a classical pushbroom technique. Le Vine et al. (2000) were able to generate an SSS map using the Electronically Steered Thinned Array Radiometer (ESTAR), the first one-dimensional synthetic aperture radiometer flown on an aircraft.

Early in the 1990s ESA started preparing the specifications for a polarimetric two-dimensional synthetic aperture radiometer, improving the ESTAR design. The result was MIRAS (Microwave Imaging Radiometer with Aperture Synthesis), with a large number of antennas along a Y-shaped 3 arms structure (Martín-Neira and Goutoule, 1997). The optimum sampling strategy of the spatial frequency plane is on a hexagonal grid, instead of the rectangular one commonly used in signal or image processing (Camps, 1996). This strategy allows an increase of the maximum antenna separation without suffering from aliasing effects in the image reconstruction process, or alternatively for the same antenna spacing enlarging the alias-free field-of-view (AF-FOV) as compared to rectangular sampling. For a given number of elements, the array structure that provides the largest spatial frequency coverage (best angular resolution) is a Y structure.

The two-dimensional MIRAS interferometer allows to measure T_B at large incidences, for two polarisations. Moreover, the instrument records instantaneously a whole scene; as the satellite moves, a given point within the 2D FOV is observed from different view angles. One then obtains a series of independent measurements, which allows retrieving surface parameters with much improved accuracy. The concept is fully scalable and allows achieving very fine spatial resolution without moving parts. A first MIRAS feasibility study was carried out by France in 1992–1996 and the development of receivers (LICEF, Lightweight Cost-Effective Front-end) was started in 1995 by Spain. In 1998 EADS-CASA Espacio took the lead of the technology development through the MIRAS Demonstrator Pilot Project. The first measurements of the MIRAS prototype led to the finding of the Corbella equation (Corbella et al., 2004) that introduced a fundamental modification in the visibility equation used in radioastronomy.

In summer 1998 ESA launched the first call for Earth Explorer Opportunity Missions within its new Living Planet program. Taking advantage of the recent technological developments, a large group of land and ocean researchers, together with microwave technologists, submitted a SMOS (Soil Moisture and Ocean Salinity) proposal (Kerr et al., 2001; Font et al., 2004). The previous year a mission using MIRAS had been proposed to the French Space Agency (CNES) under the name of RAMSES (Radiométrie Appliquée à la Mesure de la Salinité et de l'Eau dans le Sol), but although being initially selected its implementation was finally discarded. ESA considered SMOS was a risky proposal, due to its new technological concept, never flown before on a satellite, but the maturity and the innovative character of this concept, as well as the timeliness and relevance of the proposed objectives for Earth observation qualified the proposal for being selected in May 1999 as the second Earth Explorer Opportunity Mission out of 27 submitted proposals. SMOS

was established as a co-operative ESA-lead mission with contributions from the French CNES and the Spanish Center for Technological and Industrial Development (CDTI).

The initial configuration proposed an instrument working at 1.4 GHz with 25 equally spaced antenna elements in each one of its 4.5 m long arms, plus 4 additional receivers in the central hub. In order to fit in the launcher fairing, each arm was proposed to be folded in five sections in stowed configuration. The instrument would be installed on a PROTEUS generic platform provided by CNES with an antenna plane tilted 20–30° with respect to nadir to guarantee an incidence angle range within [0°, 50°]. The orbit was proposed to be sun-synchronous with Equator crossing at 6 AM (ascending) and 6 PM (descending) to minimize the perturbation on L-band signal (air, vegetation and soil temperature almost identical) and making the Faraday effect minimum. Raw measuring performances were expected to be: 30 to more than 90 km for ground resolution, 0.8–2 K for radiometric sensitivity, 1–3 days for temporal sampling, depending upon latitude, nature of the target and location within the instrument FOV.

An important aspect in the SMOS proposal was the need to use novel calibration techniques, combining both on board reference noise sources of known power level and external constant T_B targets, to ensure a high stability of the measurements. Concerning the operation mode, each 300 ms an image was to be taken, successively in horizontal and vertical polarization. The huge amount of data generated forced to propose some pre-processing on board, with averages of 5 images to obtain one to be formatted and sent to the platform. The resulting equivalent integration time is 1.5s/polarization, so 2 images are available every 3s. No mention was made by then of the possibility of full polarization capability. At the moment of preparing the proposal it was considered that the retrieval of ocean salinity required an independent measurement of sea surface temperature, to be provided through a secondary frequency. The preliminary analysis indicated that a C-band channel could potentially be useful. However, this option was soon discarded due to the mass and power limitations imposed by the use of the PROTEUS platform, suited for a minisatellite, but not allowing simultaneous operations of the two instruments.

The SMOS Phase A development started in 2000, Phase B in 2002, and Phase C/D in 2003 with a launch expected for 2007, that was later delayed until taking place in November 2, 2009. A configuration optimization analysis (Waldteufel et al., 2003) concluded, mainly driven by the more restringing soil moisture requirements in terms of resolution and coverage, that the number of elements per arm should be 21 (six on each one of three folding sections, plus three in the hub), the satellite steering angle 30°, the orbit height around 755 km, the tilt of the antenna plane close to 33°, and the spacing between antenna elements 0.875 wavelengths. During the detailed mission design it appeared that, in spite of the efforts made in successive improvements on the receivers and other components design, the PROTEUS capability was really at the limit with almost no margin, so it was decided to remove three of the receivers in the hub. The final number of antenna elements is 69 and 72 receivers, 66 LICEFs and six noise injection radiometers, are connected to them (McMullan et al., 2008).

The final configuration includes an orbit of 100 min duration with mean altitude of 758 km and inclination of 98.44°; low-Earth, polar, Sun-synchronous, quasi-circular, dusk-dawn, 149-day repeat cycle, 3-day sub-cycle. Global coverage, 80° N/S latitude, with a nominal swath of 1,050 km (3-day coverage) and narrow swath of 640 km (7-day, better radiometric accuracy and large number of incidence angles). The instrument operates at a frequency of 1,413 MHz with 1.2s integration time. Two possible observation modes are implemented: dual-polarization, where horizontal and vertical T_B are recorded in consecutive snapshots, and full-polarization, where the third and fourth Stokes parameters are also acquired in a more complex observation sequence (Martín-Neira et al., 2002). The satellite mass is 658 kg (platform: 275 kg, payload: 355 kg, fuel: 28 kg). The Data Processing Centre is at ESAC, Spain, long-term archive in Kiruna, Sweden, and User Services via ESA's Centre for Earth Observation ESRIN.

3.4.2 Key Science Requirements

SMOS is known as the ESA's Water Mission (Drinkwater et al., 2009) and its main objective is to demonstrate the feasibility of using spaceborne radiometric interferometry for Earth observation to provide global and continuous coverage of soil moisture and ocean salinity with resolution and accuracy adequate to fulfill the mission science requirements. A significant increase of the present knowledge of the spatial distribution and temporal evolution of these two geophysical variables, key to the Earth's global water cycle, is expected to improve the efficiency of our present systems for weather forecast, climate evolution analysis, prevention of natural catastrophic events impact, as well as water resources management.

For ocean salinity (Font et al., 2004), SMOS aims at meeting the salinity remote sensing objectives as defined by the Salinity and Sea Ice Working Group (Lagerloef, 2001): improving seasonal to interannual climate prediction, improving ocean rainfall estimates and global hydrologic budgets, and monitoring large scale salinity events and thermohaline convection. The mission expects being able to observe phenomena like barrier layer effects on tropical Pacific heat flux, halosteric adjustment of heat storage from sea level, North Atlantic thermohaline circulation, surface freshwater flux balance, among other relevant for large-scale and climatic studies. This requires an obtainable accuracy of 0.1–0.4 pss over 100–300 km in 10–30 days. Then the scientific requirement put to the mission was to obtain at least one mean value per 100 km square every month with an accuracy of 0.1 pss. This is a challenging requirement that may have to be relaxed depending on the finally obtained performances for the instrument and the salinity retrieval algorithm.

3.4.3 Basic SMOS Algorithm Approach

The SMOS approach to retrieve the salinity field from the reconstructed T_B images at each orbit uses the multiangular nature of the observations. Due to the shape of the FOV, as closer to the satellite sub track, a single spot in the ocean is seen in

more successive snapshots and under more different angles. A maximum of above 60 horizontal and 60 vertical T_B measurements is obtained in the centre, decreasing to half of it at 300 km to both sides. The retrieval algorithm performs a minimization loop using a cost function where the recorded T_B is compared to a T_B modeled value for each one of the available angular measurements, until an optimal fit is reached.

The forward model, or geophysical model function (GMF), that provides the T_B values corresponding to specific seawater characteristics and viewing geometry is a key component of the retrieval algorithm. It has to simulate the emission from the top ocean layer, plus any other radiation at the same frequency coming from external sources (e.g. the cosmic background) and scattered on the ocean surface to the concerned direction, and finally the transformation the overall radiation leaving the surface suffers until reaching the SMOS antenna plane (from atmosphere attenuation and upward emission until Faraday polarization rotation in the ionosphere). The emissivity of a flat sea as function of temperature, salinity, viewing angle, frequency and polarization is quite well modeled using the geometric optics theory (Klein and Swift, 1977), but the different processes that impact on the L-band emission of a roughened surface were not fully described in the several theoretical formulations available at the moment of starting the development of SMOS algorithms. It was necessary to design several new components of the GMF for the SMOS Level 2 Ocean Salinity Processor (L2OP, Zine et al., 2008).

The effect of surface roughness on the T_B is the main geophysical source of error. Unlike Aquarius, SMOS does not have any means to acquire simultaneous independent information of this roughness to be used in the GMF. In addition to this, the available data reporting rough sea surface emissivity dependencies with wind speed does not allow to discriminate the best adapted formulation among the several theoretical models proposed (Font et al., 2006). The SMOS L2OP implements the approach of the polarized ocean T_B being the addition of two terms, one corresponding to the flat sea emission and the other one a correction to it due to the impact of the surface roughness. For this correction three different options were considered, to be tested, improved or even discarded once SMOS data are available. Two of them are theoretical formulations (statistical description of the sea surface plus electromagnetic scattering model) based on the two-scale model (Dinnat et al., 2002) and the small slope approximation (Johnson and Zhang, 1999), and the third one (Gabarró et al., 2004) is an experimental fit, using different roughness descriptors, from data acquired during the WISE trials carried out as part of the SMOS science definition studies (Camps et al., 2004). All these roughness models require the use of external information on wind speed, significant wave height, wave age, etc. to describe the sea state. They are provided to the L2OP by global operational forecasts (atmospheric and ocean wave models) from the European Centre for Medium range Weather Forecasts (ECMWF) that also deliver other parameters, as sea surface temperature, needed by different modules of the retrieval algorithm. These ECMWF variables are introduced as first guess values in the cost function, and during the minimization process they are also tuned like SSS, initially obtained from climatology, until reaching the optimum fit between modeled and measured T_B. This multi-parameter convergence is possible thanks to the over-determination

produced by the existence of independent measurements (different incidence angles) of the T_B emitted by the ocean surface, which SSS does not change during the satellite overpass.

3.4.4 Expected SMOS Performance, Error Analysis

The determination of ocean salinity by SMOS has a major drawback, compared to the retrieval of soil moisture, in the much lower sensitivity of T_B to salinity changes, especially at low temperatures. This makes the instrument performance more critical for salinity retrieval. The science requirements established for the mission translated into quite strict radiometric requirements for MIRAS, but tests made after completing the instrument development indicated these were met with considerable margin. The Table 3.1 summarizes the MIRAS radiometric requirements and performances expressed in RMS of T_B as measured in May–June 2007 at the Maxwell Electromagnetic Chamber in ESTEC (European Space Technology Centre, ESA, The Netherlands). The values presented in the table provide the worst case, whenever several measurements were available (Font et al., 2010).

Besides the mentioned low range of T_B values that correspond to the whole range of salinity values in the world oceans, other key problems are impacting the quality of SMOS retrieval of ocean salinity. First, although the radiometric performance of the instrument is better than initially expected, the process of image reconstruction from the correlations of the measurements made by the individual antenna elements is introducing some errors (not well known yet) that would not exist if the measurement was directly made by a physical aperture antenna. Second, there is a need for simultaneous auxiliary information on the sea surface properties (temperature, roughness ...) to be estimated from external sources, as they are not directly measured by SMOS itself. The inaccuracy of this information (in terms of bias and noise in the auxiliary fields provided by the 3-hourly ECMWF forecasts) impacts on the retrieved salinity, in spite of these being only taken as reference values in the convergence retrieval procedure. And third, the imperfections in the different modules that constitute the GMF are also introducing degradations in the retrieval quality

Table 3.1 MIRAS system radiometric requirements and instrument-measured performances at boresight and at the edge of the FOV (32°)

	Required	Measured
Systematic error	1.5 K RMS (0°) 2.5 K RMS (32°)	0.9 K RMS in AF-FOV
Land ($T_{Bland} = 220$ K)	3.5 K RMS (0°)	2.23 K RMS (0°)
Radiometric sensitivity	5.8 K RMS (32°)	3.95 K RMS (32°)
Ocean ($T_{Bocean} = 150$ K)	2.5 K RMS (0°)	1.88 K RMS (0°)
Radiometric sensitivity	4.1 K RMS (32°)	3.32 K RMS (32°)
Stability (1.2s interval)	4.1 K RMS (<32°)	4.03 K RMS
Stability (6 d interval)	0.03 K	<0.02 K

with respect the one that would be obtained if a perfect model existed. This includes not only the mentioned problem of the surface roughness effect (how the roughness is described with the available environmental parameters and how the roughness modifies the ocean emission, with the additional impact caused by the presence of foam at high winds), but also the determination of other GMF components as the contribution to the signal of the polarized emission of galactic bodies reflected on the roughened sea surface.

The particularities of the imaging capability of an interferometric radiometer contribute to the performance of the salinity determination. We have mentioned the weakness due to the need of performing an image reconstruction step, but SMOS has remarkable strengths compared to measurements made by real aperture antennas. We have highlighted before the multi-angular observation that allows taking advantage of the sensitivity of T_B to the incidence angle to increase the robustness of the inversion. Another fundamental feature is the high angular resolution that allows imaging pixels of the order of 30 km and as a consequence identifying different elements within the FOV. This allows locating the pixels that include a direct, or more likely reflected, image of the Sun. With the SMOS orientation, the Sun is present in 97% of the snapshots; and considering the very high T_B of the Sun L-band emission, it is necessary to discard the few affected angular measurements instead of attempting a correction.

Concerning the observation modes, if MIRAS is operating in dual-polarization every 1.2 s either horizontal or vertical T_B is acquired in consecutive snapshots. Under full-polarization, some time is dedicated to acquire the cross-polarized components and then less data is available for each polarization and there is less noise reduction. However, the additional information can be used to avoid the singularities of the transformation from the antenna to the Earth reference frame, to allow improved RFI detection, to eventually identify azimuthal signals, or to estimate the Faraday rotation. Both modes are to be tested during SMOS Commissioning Phase (6 months after launch) to decide what is the nominal configuration to be used for operations. The salinity retrieval can be performed using the two polarized T_B separately or applying all the calculations to the first Stokes parameter, the sum of both polarizations. Doing the latter the number of independent measurements to integrate in the inversion is halved, then the noise reduction diminishes, but the problem of polarization mixing by Faraday rotation is avoided. Other advantages of this approach is that the uncertainties in the T_B associated to angular dependencies of the sea water dielectric constant model and in the roughness correction term are reduced, as well as the above mentioned singularities in the geometric transformation disappear.

Idealized tests of the SMOS L2OP performance have been done under different configurations and environmental conditions (Zine et al., 2008). Simulated scenes are used to compute the polarized T_B in the SMOS swath along an orbit. Then radiometric noise is added according to the expected MIRAS performance, and the processor is run with different errors and biases for the auxiliary parameters. These tests show that the retrieved SSS values from one satellite overpass will be affected by considerable noise, both from radiometric origin and from uncertainties in the

algorithm and auxiliary data. This error is of the order of 0.5–0.7 pss in the centre of the swath and degrades to about 1.5 on its borders. These results improve with high SST scenes, but can be as bad as 1.2 pss (centre) and 2.4 pss (borders) for SST = 5°C. Introducing biases on the auxiliary parameters produces also a bias on the retrieved SSS that can reach up to 0.7 pss (centre) and 0.9 pss (border) when wind speed is biased by 2 m/s. More realistic conditions (e.g. using all the measured antenna patterns for the different MIRAS elements) have been considered in some SMOS system end-to-end performance tests, and these indicate that the above described accuracy of the salinity determination can be degraded by about 50%.

It appears evident that the quality of salinity retrieval obtained from a SMOS orbit (in grid points situated in an Icosahedral Snyder Equal Area projection, ISEA4H9, 15 km characteristic length scale, as interpolated during image reconstruction) will not meet the mission scientific requirements. This is expected to be significantly improved by performing spatio-temporal averages in the generation of global gridded maps (Boutin et al., 2003). A salinity error budget analysis (Sabia et al., 2010) made in an open ocean region using different combinations of configurations and auxiliary data uncertainties, concluded that an average of SMOS products over 30 days and $2^\circ \times 2^\circ$ boxes would generate a SSS map with an error of 0.22 pss, very close to the mission requirements. In further processing steps this can be improved by introducing balancing terms in the cost function (Gabarró et al., 2009) and by bias reduction through external calibration techniques using other sources of salinity data.

3.5 Aquarius/SAC-D Mission

3.5.1 Early Configuration and Evolution of Design

The first significant step toward a NASA salinity mission began with the Salinity Sea Ice Working Group (SSIWG), established in early 1998. The SSIWG included participation from United States as well as European scientists and engineers. During that year the SMOS mission was also being formulated for proposal to ESA (see above). The SSIWG became an international, voluntary and open forum, and held workshops in 1998, 1999 and 2000 focusing on a range of scientific and technical issues covered by the charter (see www.esr.org/ssiwg/mainssiwg.html). The SSIWG provided the basic scientific framework and objectives for salinity remote sensing and outlined basic measurement requirements (Lagerloef et al., 2008). An analyses by Yueh et al. (2001) provided more rigorous assessment of the technical issues and feasibility. During this time, parallel efforts continued in both Europe (with SMOS) and in the United States. The NASA effort focused on satellite sensor concepts and mission designs to measure salinity as a primary objective. Another team in the US pursued a separate mission concept to measure soil moisture with science requirements that demanded much higher spatial and temporal resolution, but much less radiometric accuracy, than needed for salinity.

In 2000, NASA was preparing to release an Announcement of Opportunity (AO) for the Earth System Science Pathfinder (ESSP) program. That same year, the Goddard Space Flight Center (GSFC) and Jet Propulsion Laboratory (JPL) agreed to develop jointly an ESSP mission concept and proposal for an Ocean Salinity Measurement Mission (OSMM). They considered 3 mission concepts, including a (1) single large aperture feed horn, (2) a three-beam pushbroom design, and (3) a conically scanning antenna system. In December, 2000, the 3-beam pushbroom concept was selected after considerable technical evaluation. This offered the best trade-offs between system accuracy, sampling statistics and engineering complexity.

In January 2001, the OSMM concept was named *Aquarius* after the celestial constellation of the same name. In ancient middle-east mythology, Aquarius was the water-bearer whose appearance coincided with the rainy season, and in ancient Egypt, the flooding of the Nile. The image is of a man pouring water on the earth from a large urn. It is a suitable name for an earth science mission to explore how the water cycle, ocean circulation and climate interact in an era of likely anthropogenic climate change. The Aquarius Step 1 (science and mission concept) proposal was submitted to NASA in July 2001 under the ESSP AO. Of the 18 Step 1 proposed ESSP missions, Aquarius and five others were selected to proceed with a Step 2 (technical implementation and cost) proposal.

In November 2001, the Aquarius team agreed with the Argentina Comisión Nacional de Actividades Espaciales (CONAE) to propose a joint mission for Step 2. CONAE would furnish the satellite, mission operations and complementary sensors at no cost to NASA. The mission would become the fourth Satélite de Aplicaciones Científicas (SAC) developed by Argentina in partnership with the US. The SAC-D science objectives are local measurements over Argentina and contribute to global investigations of atmosphere, oceans and effects of human and natural processes on the environment, as per the Argentine National Space Program strategic plan.

The Aquarius NASA proposal was to provide the salinity sensor, science, launch vehicle and other implementation costs. The Step 2 proposal was completed in January 2002, and Aquarius was selected in July 2002 as one of two primary missions to proceed with further definition studies, along with one alternate. The project was then directed to do a 1-year risk reduction study, during which time the NASA-CONAE team re-configured the observatory design to allow CONAE and third party instruments to be included and resembles the final configuration we have today (Fig. 3.4). The mission formulation phase (Phase B) began in December 2003, leading to the system requirements reviews in August and September 2004, and preliminary design reviews in June–August 2005. The NASA mission confirmation review in September 2005 marked the start of the implementation phase (Phase C/D). The joint NASA-CONAE mission critical design review took place in Buenos Aires, July 2008, and the present launch date is scheduled for autumn 2010.

A schematic of the mission profile is shown in Fig. 3.5. The design incorporates several key functional elements. The pushbroom footprint pattern has a $\sim$390 km wide swath consisting of 3 elliptical beam footprints of sizes 76 km $\times$ 94 km, 84 km $\times$ 120 km and 96 km $\times$ 156 km. The measurements will be relatively low spatial resolution, as was stressed in Lagerloef et al. (1995, 2008) and most suited

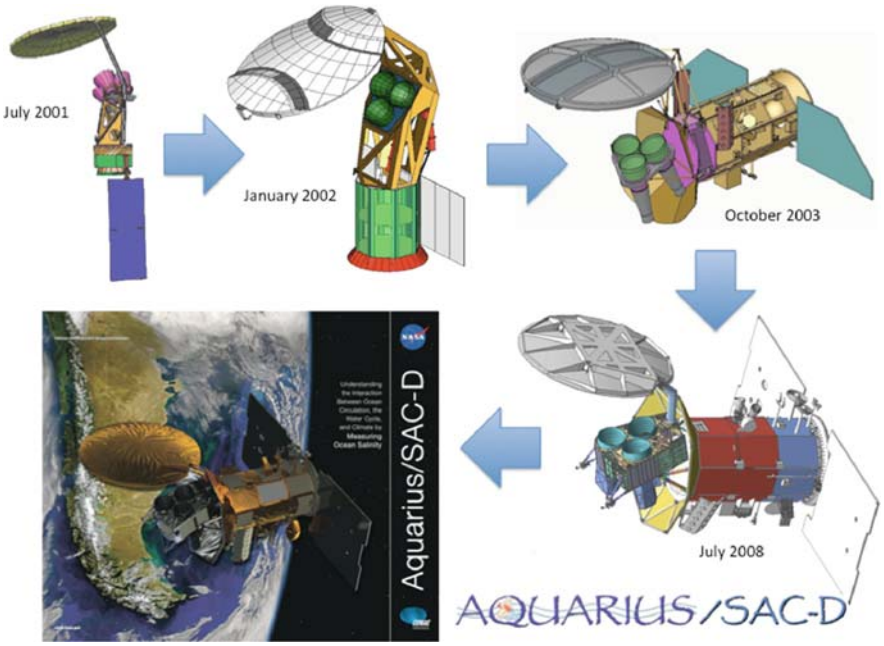

Fig. 3.4 The evolution of the Aquarius/SAC-D mission design: Step 1 Proposal (July 2001); Step 2 Proposal (January 2002); After reconfiguration design (October 2003); Mission Critical Design Review (July 2008); Artist concept of on-orbit observatory over Patagonia

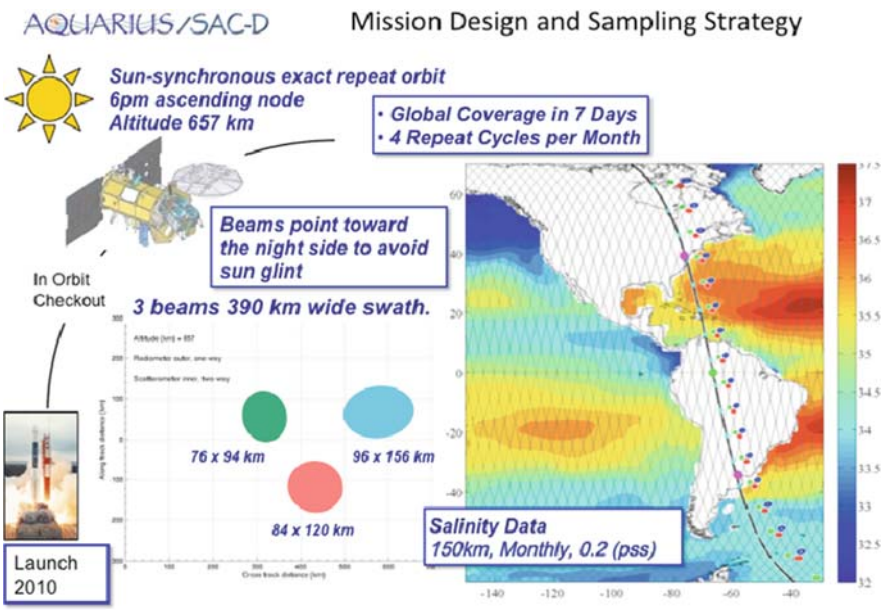

Fig. 3.5 A schematic of the Aquarius/SAC-D mission profile, showing the 3-beam push broom swath (*center*) and the approximate orbit geometry over the western hemisphere (*right*)

for resolving the basin scale SSS field. This will filter much of the eddy and frontal scales, yet provide much greater detail than is derived from historical data (World Ocean Atlas 2005), as illustrated by Lagerloef et al. (2008). The three Aquarius microwave radiometers will measure microwave brightness temperature in vertical and horizontal polarizations (T_{BH} and T_{BV} respectively), as well as polarimetric channels to correct for the Faraday rotation of the signal as it passes through the ionosphere (Yueh, 2000). These sensors are aligned with an offset 2.5 m aperture antenna reflector to generate the 3 fixed beams at incidence angles of 28.7, 37.8 and 45.6° relative to the ocean surface and form the 3 distinct footprints aligned across the swath (more technical details in Le Vine et al., 2007). The Aquarius microwave radiometers have very demanding requirements for low noise and calibration stability, and will be the most accurate ever developed for Earth remote sensing.

The satellite will be placed in a sun-synchronous polar orbit crossing the equator northward (ascending) at 6 PM. The sensor will be viewing away from the sun to avoid solar contamination of the science measurement. The 7-day repeat orbit track spacing at the equator is equal to the swath width. This ensures that the sampling pattern gives total area coverage (no significant swath gaps) and sufficient repeat observations to allow the errors to be reduced by monthly averages. The primary Aquarius microwave sensor combines an L-band microwave radiometer of unprecedented accuracy with an integrated L-band radar to provide a measurement correction for surface roughness, which as noted above, is the significant error source.

The CONAE Microwave Radiometer (MWR) will make complementary measurements of rain, wind and sea ice with 23.8 and 36.5 GHz channels in an overlapping swath pattern (Lagerloef et al., 2008). The MWR data will be used by the Aquarius data processing for rain and sea ice flags, and as supplementary rain and surface wind speed correction algorithms. The New InfraRed Scanner Technology (NIRST) camera is a narrow swath imager intended to detect forest fires and other thermal events on land. It can be tilted to observe preferred targets, and on occasion will be used to map SST within one Aquarius footprint.

3.5.2 Key Science Requirements

The principal scientific requirement is to make global SSS measurements over the open oceans with 150 km spatial resolution, and to achieve a measurement error less than 0.2 (pss) on a 30 day time scale, taking into account all sensor and geophysical random errors and biases. For comparison, the Global Ocean Data Assimilation Experiment (GODAE) requirement is one sample every 10 days/200 km^2 and SSS error of 0.1. Presently, the Global Ocean Observing System (GOOS) provides about 40% of this global sampling (exclusive of the sea ice covered regions and continental shelf) with in-situ observations (principally Argo). The requirement applies to the open ocean, sufficiently far from land or ice boundaries so that the warmer land and ice brightness temperatures, as compared to the ocean surface, do not contaminate the radiometric measurement. Generally this boundary zone is about 2–3 times the footprint diameter. The baseline mission is designed to operate for up to 3 years, with potential extended durations for 2 years or longer.

3.5.3 Basic Aquarius Algorithm Approach

The Aquarius retrieval algorithm is being developed using very thorough simulation to test and quantify errors in the retrievals prior to launch. Starting with the dielectric model of equations (3.1) and (3.2), the Aquarius science simulator generates a forward computation of the top of the atmosphere brightness temperatures based on an ocean model SSS and SST field. The simulator adds all the geophysical radiative sources described in Section 3.3, convolves the Aquarius antenna gain patterns and thus derives the brightness temperature input to the three individual radiometers (called antenna temperatures). Estimated errors for the sensor and geophysical corrections are added, and then the inverse calculation is performed to compare with the input SSS field. A 30-day simulation and retrieval analysis shows worst-case salinity errors ~0.5 in high latitudes and <0.2 in the latitude range 40N–40S for point measurements (5.76s integration time), which would be further reduced by monthly averaging. See also Lagerloef et al. (2008, 2010) and Kim et al. (2010) for more simulator details. A new 1-year simulation is now being computed and will be available at the time of the Oceans from Space 2010 meeting.

The Aquarius baseline retrieval algorithm utilizes both polarization channels in the basic retrieval model (Lagerloef et al., 2008)

$$S = a_0 + a_1 T_V + a_2 T_H + a_3 W + ... \tag{3.3}$$

The coefficients a_0, a_1, a_2 and a_3 are independent functions of SST and the individual beam incidence angle θ. These are presently derived by regression analysis with the simulated data and will be tuned with surface calibration during the mission. The sensitivity to wind roughness is less for T_V than for T_H, (Camps et al., 2004). This allows the possible tuning of the coefficients a_1 and a_2 to off set the roughness effect to some degree. W represents an independent wind parameterization which can be input based on the radar scatterometer data or from an ancillary data source. The present simulator uses ancillary wind fields, and the "at launch" processor will do likewise, until both the radiometer and radar sensors have been calibrated in-orbit and the correction algorithms tuned accordingly. The model can also be expanded to include non-linearities and additional ancillary terms such as wave height, rain rate or wind direction.

3.5.4 Expected Aquarius/SAC-D Performance, Error Analysis

A careful error analysis has been maintained for the Aquarius measurement system throughout the design and construction phase. This includes the measurement errors inherent in the sensor (NEDT noise and calibration stability), the roughness correction retrieval error from the radar, and a residual uncertainty from number of geophysical error sources based on the maturity of the models and the uncertainties in the associated ancillary data. Error terms are tabulated based on an individual

observation consisting of a 5.76s data integration along track for each of the 3 Aquarius radiometer beams. The allocation is given in Table 3.2, where the sources are combined as a root sum square. Both the allocation and the current best estimate (CBE) are shown, and the margin is defined as the additional rss error that could

Table 3.2 Top portion shows the allocated sensor and geophysical errors (left column) in terms of v-polarized brightness temperature (T_{BV}) in Kelvin (K), and the Current Best Estimate (CBE) (right column) for each measurement with 5.76s integration time. The radiometer CBE data are based on the Aquarius instrument pre-launch calibration data. The margin is the additional RSS error that could be included before exceeding the allocation. Bottom portion shows the monthly RMS salinity error by latitude band based on the total error allocation of 0.38 K per sample. These include the measurement sensitivity as it varies with SST and the number of samples averaged per latitude band. The global RMS error allocation over all the latitude bands is 0.2 and CBE 0.15 (pss)

	3 beam RMS (K)	
Error sources	Allocation	CBE
Radiometer	0.15	0.13
Antenna	0.08	0.01
System pointing	0.05	0.02
Roughness	0.28	0.13
Solar	0.05	0.02
Galactic	0.05	0.04
Rain (Total liquid water)	0.02	0.01
Ionosphere	0.06	0.05
Atmosphere – other	0.05	0.02
SST	0.10	0.07
Antenna gain near land & ice	0.10	0.10
Model function	0.08	0.07

	Baseline mission 3 beams RMS (K)	
Brightness temperature error per observation	Allocation	CBE
Total RSS (K)	0.38	0.24
Margin RSS (K)	0.30	

			Baseline mission monthly salinity error (psu)	
Latitude range	Mean sensitivity (dTv/dS)	Mean # samples in 28 days	Allocation	CBE
0–10	0.756	10.9	0.15	0.10
11–20	0.731	11.3	0.16	0.10
21–30	0.671	12.1	0.16	0.10
31–40	0.567	13.5	0.18	0.12
41–50	0.455	15.9	0.21	0.13
51–60	0.357	20.3	0.24	0.15
61–70	0.271	30.2	0.26	0.16
Global RMS (pss)			0.20	0.13
Margin RSS (pss)			0.15	

be added to the CBE without exceeding the allocation. Table 3.2 also provides the separation of monthly average error by latitude range, according to the prevailing sea surface temperature. As noted earlier, the sensitivity decreases as temperature decreases, increasing the errors in higher latitudes.

The sample rate increases in higher latitudes from the polar orbiting orientation of the satellite, which is reflected in the mean number of samples per month shown in the table. The largest single error source in the table is the roughness effect due to wind and waves, as described above, and is the reason why the Aquarius instrument includes an integrated L-band (1.26 GHz) radar scatterometer to measure simultaneous oceanic backscatter in the footprint as noted above. The Aquarius roughness error allocation is presently based on limited airborne radiometer and radar combined measurements (Wilson et al., 2001) and is expected to improve with additional airborne data collected in March 2009, which are still being analyzed. More improvements will be derived once the satellite is on orbit. The remaining geophysical error sources are the estimated uncertainty residuals after the best known correction models have been applied. The degree of understanding has been the result of rigorous studies of the ionosphere, galactic reflections, sun and so forth (Le Vine and Abraham, 2002, 2004; Le Vine et al., 2005).

The estimates in Table 3.2 are based on the assumption that all the errors are uncorrelated. In nature, some of these errors are likely to exhibit long correlation scales, especially among the various geophysical effects, and with slow variations in the sensor calibration. The assumptions are tested with the Aquarius science simulator as noted above. Those results, also shown in Lagerloef et al. (2008, 2010), indicate retrieval errors within the science requirement of 0.2 pss monthly average with substantial margin.

3.6 Summary: A Look to the Future Follow-on Possibilities

The simultaneous flights of SMOS and Aquarius/SAC-D give the oceanographic community a rare opportunity to test and evaluate two very different technical approaches: phased-array versus real aperture radiometry. In addition, Aquarius will be the first L-band integrated passive-active (radiometer and radar scatterometer) sensor in space, providing added value for land and ice data analysis as well. Both missions, as pathfinders, have as part of their objectives to demonstrate the technical feasibility and scientific value of the data as a foundation for future salinity missions. Also, as pathfinders, they do not try to do too much – the focus is to provide rather coarse resolution averaged data, consistent with climatological scales (~100–200 km, monthly), for the open ocean and removed from land and ice boundaries.

Once SSS measurements on these scales are demonstrated, calibrated and validated, the demand will grow to obtain ~10 km resolution, near coastal measurements and higher accuracy. The higher spatial resolution and near-coast measurement issues can only be solved by flying ~25 m aperture antennas. Will phased-array or real-aperture be the optimal approach? Can radiometric accuracy

<0.1 K be achieved with such large hardware dimensions? These are the types of over-arching technical challenges for the future, for which SMOS and Aquarius will provide vital technical data to consider the best options.

The other key consideration for future missions, of course, is data continuity. Aquarius and SMOS will provide unprecedented benchmark measurements of an essential climate variable at a time when the planet appears to be experiencing dramatic climate change. As we analyze the satellite SSS data in the next few years, the scientific benefit and need to maintain a climate data record for decades to come will become obvious.

Two opportunities for SSS measurement continuity beyond SMOS and Aquarius/SAC-D are likely. ESA has begun considering possible improvements on the basic MIRAS design to propose a series of operational satellites (SMOSops, SMOS Operational System) that could follow SMOS with similar characteristics. Options are also being studied to augment MIRAS to provide a simultaneous roughness measurement. Several preparatory studies have been carried out in 2007–2008 to analyze some of these possible improvements, although no decision will be taken until an evaluation of the SMOS mission achievements can be made.

In the United States, NASA is developing the Soil Moisture Mapping mission (SMAP) for possible launch in 2015. This is a conically scanning system with a large 6 m offset mesh antenna with a radiometer footprint size of ~40 km. It offers the only viable option in NASA for follow-on salinity measurements, although it is primarily designed for soil moisture measurement. Like Aquarius, SMAP will have an integrated L-band radiometer and radar sensor which will provide simultaneous brightness and roughness measurements over the ocean. The sample rate will be much higher than for Aquarius, although the radiometric accuracy will not be as good. A simulation study is planned for early 2010 to analyze how well the SMAP design could perform to meet the Aquarius science measurement requirements.

We believe that Oceans from Space 2010 is witness to the start of a new era in ocean remote sensing; one that will include ocean salinity as a fully functional component of the array of space borne ocean measurements. The next decade will bring important new discoveries and oceanographic insights. What shall we wager for Oceans from Space 2020 regarding ocean salinity? Will we have a decade of satellite SSS data to analyze? Will ENSO forecast skill be measurably improved as a result? Will the global marine freshwater balance be known to within a few percent? Will upper ocean mixing process be much better understood as a result, and new parameterizations be imbedded in our best ocean general circulation and climate models? Will we have found some significant ocean features and phenomena that we did not anticipate? All of these speculations are certainly worth about ½ pinch of salt in a bottle of wine.

Acknowledgements This chapter is partly a contribution to the SMOS Barcelona Expert Centre on Radiometric Calibration and Ocean Salinity (SMOS-BEC) funded through grant ESP2007-05667-C04 from the Spanish Ministry of Science and Innovation.

References

Blanch S, Aguasca A (2004) Seawater dielectric permittivity model from measurements at L-band. Paper presented at International Geoscience and Remote Sensing Symposium IGARSS, 20–24 September 2004

Boutin J, Waldteufel P, Martin N, Caudal G, Dinnat EP (2003) Surface salinity retrieved from SMOS measurements over the global ocean: imprecisions due to sea surface roughness and temperature uncertainties. J Atmos Ocean Technol 21:1432–1447

Broecker WS (1991) The great ocean conveyor. Oceanography 4:79–89

Camps A (1996) Application of interferometric radiometry to Earth observation. PhD Thesis, Univ Politècnica de Catalunya, http://www.tdx.cesca.es/TDX-1020104-091741/

Camps A, Font J, Vall-llossera M, Gabarró C, Corbella I, Duffo N, Torres F, Blanch S, Aguasca A, Villarino R, Enrique L, Miranda J, Arenas J, Julià A, Etcheto J, Caselles V, Weill A, Boutin J, Contardo S, Niclós R, Rivas R, Reising SC, Wursteisen P, Berger M, Martín-Neira M (2004) The WISE 2000 and 2001 field experiments in support of the SMOS mission: sea surface L-band brightness temperature observations and their application to multi-angular salinity retrieval. IEEE Trans Geosci Rem Sens 42:804–823

Corbella I, Duffo N, Vall-llossera M, Camps A, Torres F (2004) The visibility function in interferometric aperture synthesis radiometry. IEEE Trans Geosci Rem Sens 42:1677–1682

Dinnat EP, Boutin J, Caudal G, Etcheto J, Waldteufel P (2002) Influence of sea surface emissivity model parameters at L-band for the estimation of salinity. Int J Remote Sens 23:5117–5122

Drinkwater M, Kerr YH, Font J, Berger M (2009) Exploring the water cycle of the blue planet: the soil moisture and ocean salinity (SMOS) mission. ESA Bull 137:6–15

Ellison W, Balana A, Delbos G, Lamkaouchi K, Eymard L, Guillou C, Prigent C (1998) New permittivity measurements of sea water. Radio Sci 33(3):639–648

Font J, Lagerloef GSE, Le Vine DM, Camps A, Zanifé OZ (2004) The determination of surface salinity with the European SMOS space mission. IEEE Trans Geosci Rem Sens 42: 2196–2205

Font J, Boutin J, Reul N, Waldteufel P, Gabarró C, Zine S, Tenerelli J, Petitcolin F, Vergely JL (2006) An iterative convergence algorithm to retrieve sea surface salinity from SMOS L-band radiometric measurements. Proceedings of the IEEE International Geoscience and Remote Sensing Symposium 2006 (IGARSS 2006), Denver, pp. 1697–1701

Font J, Camps A, Borges A, Martín-Neira M, Boutin J, Reul N, Kerr YH, Hahne A, Mecklenburg S (2010) SMOS: the challenging sea surface salinity measurement from space. Proc IEEE (in press)

Gabarró C, Font J, Camps A, Vall-llossera M, Julià A (2004) A new empirical model of sea surface microwave emissivity for salinity remote sensing. Geophys Res Lett 31(L0):1309, doi:10.1029/2003GL018964

Gabarró C, Portabella M, Talone M, Font J (2009) Towards an optimal SMOS ocean salinity inversion algorithm. IEEE Trans Geosci Rem Sens 6:509–513

Gordon AL, Giulivi CF (2008) Sea surface salinity trends over 50 years within the Subtropical North Atlantic. Oceanography 21:20–29

Hakkinen S, Rhines PB (2009) Shifting surface currents in the northern North Atlantic Ocean. J Geophys Res 114(C04005), doi:10.1029/2008JC004883

Hollinger JP (1971) Passive microwave measurements of sea surface roughness. IEEE Trans Geosci Electron GE-9(3):165–169

Holliday NP, Hughes SL, Bacon S, Beszczynska-Modieller A, Hansen B, Lavín A, Loeng H, Mork KA, Østerhus S, Sherwin T, Walczowski W (2008) Reversal of the 1960s to 1990s freshening trend in the northeast North Atlantic and Nordic Seas. Geophys Res Lett 35(L03614), doi:10.1029/2007GL032675

IPCC (2007) Climate change 2007: the physical science basis. In: Solomon S, Qin D, Manning M, Chen Z, Marquis M, Avery KB, Tignor M, Miller HL (eds.) Fourth assessment report, Cambridge University Press, Cambridge, UK, pp. 996

Johnson JT, Zhang M (1999) Theoretical study of the small slope approximation for ocean polarimetric thermal emission. Wave Random Complex 37:2305–2316

Kerr YH, Fukami K, Skou N, Srokosz MA, Lagerloef GSE, Goutoule JM, Le Vine DM, Martín-Neira M, Marczewski W, Laursen B, Gazdewich J, Barà J, Camps A (1995) Proceedings of the Consultative Meeting on Soil Moisture and Ocean Salinity Measurement Requirements and Radiometer Techniques (SMOS), ESA WPP-87, ESTEC, Noordwijk, The Netherlands

Kerr YH, Waldteufel P, Wigneron JP, Martinuzzi JM, Font J, Berger M (2001) Soil moisture from space: the soil moisture and ocean salinity (SMOS) mission. IEEE Trans Geosci Rem Sens 39:1729–1735

Kim SB, Wentz F, LeVine D, Lagerloef GSE (2010) Simulation of sea surface salinity retrieval with the Aquarius L-band radiometer. IEEE Trans Geosci Rem Sens (in press)

Klein LA, Swift CT (1977) An improved model for the dielectric constant of sea water at microwave frequencies. IEEE J Ocean Eng 2:104–111.

Lagerloef GSE, Swift C, Le Vine D (1995) Sea surface salinity: the next remote sensing challenge. Oceanography 8:44–50

Lagerloef GSE (2001) Satellite measurements of salinity. In: Steele J, Thorpe S, Turekian K (eds.) Encyclopedia of Ocean Sciences, Academic Press, London, pp. 2511–2516

Lagerloef GSE (2002) Introduction to the special section: the role of surface salinity on upper ocean dynamics, air sea interaction and climate. J Geophys Res 107(C12):8000, doi:10.1029/2002JC001669

Lagerloef GSE, Colomb F, Le Vine D, Wentz F, Yueh S, Ruf C, Lilly J, Gunn J, Chao Y, deCharon A, Feldman G, Swift C (2008) The Aquarius/SAC-D mission: designed to meet the salinity remote-sensing challenge. Oceanography 20:68–81

Lagerloef G, Boutin J, Chao Y, Delcroix T, Font J, Niiler P, Reul N, Riser S, Schmitt R, Stammer D, Wentz F (2010) Resolving the global surface salinity field and variations by blending satellite and in situ observations. In: Hall J, Harrison DE, Stammer D (eds.) Proceedings of OceanObs'09: Sustained Ocean Observations and Information for Society (Vol. 2), Venice, Italy, 21–25 September 2009, ESA Publication WPP-306

Lang RH, Tarkocin Y, Utku C, Le Vine DM (2008) Recent results on the accurate measurements of the dielectric constant of seawater at 1.413 GHz. Geoscience and Remote Sensing Symposium. IGARSS 2008. IEEE International, Vol. IV, Boston, MA, pp. 950–953

Le Vine DM, Zaitzeff JB, D'Sa EJ, Miller JL, Swift C, Goodberlet M (2000) Sea surface salinity: toward an operational remote-sensing system. In: Halpern D (ed.) Satellites, Oceanography and Society, Elsevier Oceanography Series 63, Amsterdam, pp. 321–335

Le Vine DM, Lagerloef GSE, Colomb R, Yueh S, Pellerano F (2007) Aquarius: an instrument to monitor sea surface salinity from space. IEEE Trans Geosci Rem Sens 45: 2040–2050

Le Vine DM, Abraham S (2002) The effect of the ionosphere on remote sensing of sea surface salinity from space: absorption and emission at L-band. IEEE Trans Geosci Rem Sens 40:771–782

Le Vine DM, Abraham S (2004) Galactic noise and passive microwave remote sensing from space at L-band. IEEE Trans Geosci Rem Sens 42:119–129

Le Vine DM, Abraham S, Wentz F, Lagerloef GSE (2005) Impact of the sun on remote sensing of sea surface salinity from space. Proc Internat Geosci Rem Sens Symp 1:288–291, doi:10.1109/IGARSS.2005.1526164

Martín-Neira M, Goutoule JM (1997) A two-dimensional aperture-synthesis radiometer for soil moisture and ocean salinity observations. ESA Bull 92:95–104

Martín-Neira M, Ribó S, Martín-Polegre AJ (2002) Polarimetric mode of MIRAS. IEEE Trans Geosci Rem Sens 40:1755–1768

McMullan KD, Brown MA, Martín-Neira M, Ritts W, Ekholm S, Marti J, Lemanczyk J (2008) SMOS: the payload. IEEE Trans Geosci Rem Sens 46:594–605

Meissner T, Wentz FJ (2003) The complex dielectric constant of pure and sea water from microwave satellite observations. IEEE Trans Geosci Remote Sens 42:1836–1849

Ruf CS, Swift CT, Tanner AB, Le Vine DM (1988) Interferometric synthetic aperture microwave radiometry for the remote sensing of the Earth. IEEE Trans Geosc Rem Sens 26: 597–611

Sabia R, Camps A, Talone M, Vall-llossera M, Font J (2010) Determination of the sea surface salinity error budget in the soil moisture and ocean salinity mission. IEEE Trans Geosci Rem Sens doi: 10.1109/TGRS.2009.2034648

Stott PA, Sutton RT, Smith DM (2008) Detection and attribution of Atlantic salinity changes. Geophys Res Lett 35:L21702, doi:10.1029/2008GL035874

Stogryn A (1997) Equations for the permittivity of sea water. GenCorp, Aerojet Electron Syst Rep, Azusa, CA

Swift CT, McIntosh RE (1983) Considerations for microwave remote sensing of ocean-surface salinity. IEEE Trans Geosci Rem Sens 21:480–491

US CLIVAR Salinity Working Group (2007) Report of the US CLIVAR Salinity Working Group. US CLIVAR Report No. 2007-1, US CLIVAR Office, Washington, DC, available online at: http://www.sclivar.org/Pubs/Salinity_final_report.pdf

Waldteufel P, Boutin J, Kerr YH (2003) Selecting an optimal configuration for the soil moisture and ocean salinity mission. Radio Sci 38:8051

Wilson W, Yueh S, Dinardo SJ, Chazanoff S, Kitiyakara A, Li FK, Rahmat-Samii Y (2001) Passive Active L- and S-band (PALS) microwave sensor for ocean salinity and soil moisture measurements. IEEE Trans Geosci Remote Sens 39:1039–1048

Wilson WJ, Yueh S, Dinardo SJ, Li FK (2004) High-stability L-band radiometer measurements of saltwater. IEEE Trans Geosci Remote Sens 42:1829–1835

Yueh SH (2000) Estimates of faraday rotation with passive microwave polarimetry for microwave remote sensing of earth surfaces. IEEE Trans Geosci Rem Sens 38(5):2434–2438

Yueh SH, West R, Wilson WJ, Li FK, Njoku EG, Rahmat-Samii Y (2001) Error sources and feasibility for microwave remote sensing of ocean surface salinity. IEEE Trans Geosci Rem Sens 39:1049–1060

Zine S, Boutin J, Font J, Reul N, Waldteufel P, Gabarró C, Tenerelli J, Petitcolin F, Vergely JL, Talone M, Delwart S (2008) Overview of the SMOS sea surface salinity prototype processor. IEEE Trans Geosci Rem Sens 46:621–645